Waveguide fabrication using the Heidelberg MLA150 Maskless Aligner

Report submitted to the Stanford Nanofabrication Facilities in partial fulfillment of course requirements for ENGR 241.

Winter 2019

Payton Broaddus
Department of Electrical Engineering

Aditi Datta
Department of Materials Science and Engineering

Stanford University

March 2019

EXECUTIVE SUMMARY

The purpose of this document is to summarize the milestones we have achieved in the two quarter long course ENGR 241.The initial aim of our project was to develop a process flow for rapid prototyping of waveguides with acceptable losses using a direct write lithography tool and to build software for analyzing roughness parameters of the waveguides we fabricate.

So far, no comprehensive study for fundamental limitations of the Heidelberg MLA150 for the SNF in terms of resolution and actual write pattern has been done. When people begin working on the MLA150 they might have a number of questions. What sort of minimum trenches or ridges can I achieve with this tool? When I designed curved or angled lines how are these actually exposed on the wafer? What is the variability of these small features over long distances? Is there a way to reduce this? What is sort of line edge roughness occurs upon exposure? Are there ways to improve the resolution of ridges or trenches? Our project hopes to answer the above questions.

The motivation for this project comes from the disadvantages with current photolithographic techniques in the SNF in the production of waveguides. Currently, large optical networks are only possible at the SNF with masked lithography, which has a number of disadvantages involving cost, turnaround time, and limitations in design flexibility once a mask has been ordered.
The Heidelberg as an alternative option for waveguide creation boasts a number of clear advantages: maskless has no cost and no turnaround time. This would be of great benefit to the photonics community within the SNF, who could prototype and test semi-lossy photonic structures with the Heidelberg before ordering and producing high quality waveguides and photonic structures with masked photolithography.

Fall quarter we produced an SOP for finding the dose defocus pair for an arbitrary material stack. We also created an SOP for characterizing the line profile of angled ridges in order to generating the line edge roughness RMS and line width roughness RMS. We applied this SOP to optimize dose/defocus and find the line width and line edge roughness for angled ridges of Shipley 1um 3612 photoresist on a plain silicon wafer (L-prime).

This quarter we applied the SOP we developed in the fall quarter to our waveguide material stack(silicon nitride on silicon oxide) to optimize dose/defocus specific to it. We found the roughness of rings fabricated with the optimized dose/defocus without reflow and after reflowing at various times and temperatures to identify the change in line edge roughness and line width roughness. Reflow at high temperatures only seemed to increase line edge roughness and line width roughness. However, low temperature long time reflows didn’t increase the roughness, opening up the possibility to increase trench resolution at the expense of ridge resolution.

Finally, we etched, oxide capped, laser diced and polished straight silicon nitride waveguides. Once polished, we coupled 1.55um light in and extracted the loss from these straight waveguides. This report includes a number of key details in producing waveguides, as well as a general estimate for the losses the Heidelberg defined waveguides will produce.

ACKNOWLEDGEMENTS

We would like to thank our SNF mentors Swaroop Kommera and J.Provine, Professor Roger Howe and Professor Jonathan Fan, ENGR 241 classmates SNF Staff and industry mentors and TA Charmaine Chia. We would also like to thank Dr. Carston Langrock for his critical support in helping polish and characterizing our waveguides. Thank you for the constant support, valuable feedback and insightful questions throughout the quarter.

TABLE OF CONTENTS

1.BACKGROUND

1.1 CHALLENGES OF TRADITIONAL LITHOGRAPHY AND OUR SOLUTION

Traditional photolithography is an expensive and time-consuming process that is unsuitable for rapid prototyping due to the limitation of having a fixed pattern in a photomask. The Heidelberg MLA 150 Maskless Aligner is a high speed direct write lithography tool, that we use to overcome the constraints described, for the purpose of waveguide fabrication. The system exposes patterns from a CAD layout directly to a resist coated substrate without the need for a physical photomask, using a 405nm laser modulated by a digital micromirror device. This allows for quick implementation of design changes, making it well suited for rapid prototyping and iterative modification at a relatively low cost. It is typically used to produce structures down to 1μm.

1.2 BASICS OF ROUGHNESS

Infrared (IR) on-chip waveguides require smooth micron resolution strips with sub micron (>100 nm) roughness in order to meet loss requirements (>10db/cm). Roughness has two components, Line Edge Roughness (LER) which is defined as the roughness of a single printed pattern edge of the waveguide, and Line Width Roughness (LWR) which is the fluctuation in the physical distance between two printed pattern edges of the waveguide.
Line Edge Roughness in waveguides comes from the etching process in which striations on the photoresist (PR) sidewall due to intrinsic resist roughness cause pattern transfer down to the layer being etched. Smooth PR sidewalls can still cause rough etched sidewalls, a result of ion bombardment roughening [1]. However, rough PR sidewalls will almost always produce rough etches as a result of pattern transfer.

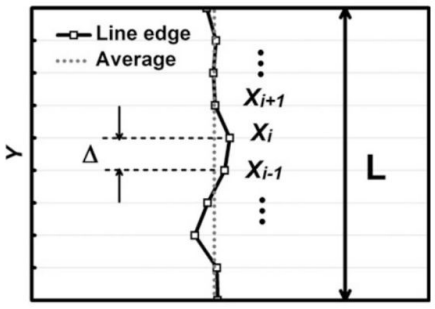

EQUATIONS USED TO CALCULATE LER AND LWR

$$\bar{x} = \left(\sum_{i=1}^{N} x_i\right) \Big/ N \quad \sigma_{\mathrm{LER}} = \sqrt{\frac{1}{N}\sum_{i=1}^{N} (\delta x_i)^2} = \sqrt{\frac{1}{N}\sum_{i=1}^{N} (x_i - \bar{x})^2} \quad (1)$$

$$\bar{w} = \left(\sum_{i=1}^{N} w_i\right) \Big/ N. \quad \sigma_{\mathrm{LWR}} = \sqrt{\frac{1}{N}\sum_{i=1}^{N} (\delta w_i)^2} = \sqrt{\frac{1}{N}\sum_{i=1}^{N} (w_i - \bar{w})^2} \quad (2)$$

$$w_i = x_i^{\mathrm{R}} - x_i^{\mathrm{L}}, \quad (3)$$

Figure 1: Example of LER

1.3 LITERATURE ON REFLOW TO REDUCE ROUGHNESS PARAMETERS ON WAVEGUIDES

Scattering due to sidewall roughness is the main source of propagation losses in waveguides. Many methods of reducing sidewall roughness have been explored such as anisotropic wet etching and thermal oxidation. Reduction of waveguide sidewall roughness by thermally reflowing the photoresist patterns to reduce their roughness to minimise the roughness transfer during etching has been proposed and demonstrated before. When the photoresist is heated above its glass transition temperature it begins to softens and spreads laterally resulting in a dome shaped profile that is smoother than the starting rectangular profile that is patterned. The roughness of a photoresist pattern is specific to its chemistry. Porklab et al.[3] have reported low loss AlGaAs waveguides using plasma assisted resist reflow. In the method described by them application of plasma to the pattern during simultaneous heating helps to reduce the lateral spreading of the photoresist patterns. The method of roughness reduction of photoresist reflow has been explored for many applications like gate fabrication for transistors[9] and for making microdisks[8] and microlens arrays[10].

1.4 SYSTEM OVERVIEW - HEIDELBERG MLA150 MASKLESS ALIGNER

The MLA150 system consists of the following individual components and their main subcomponents:

- Lithography Unit
  - Flow Box
  - Optics System
  - Granite Construction
- Electronics Rack
  - User PC with Conversion
  - Power Supply and Emergency Stop Module
  - Stage Controller
  - STC-Rack
  - Integrated Network Hub
  - Stage and Laser Chiller
- Cooling water supply
- Operator workstation

The housing of the lithography system is called the Flow Box. It provides a stable environment for constant exposure conditions by maintaining temperature laminar flow of clean air.
The system is controlled by the user using a graphical user interface on the User PC.
The optics system is comprised of a laser unit with optical elements for beam guidance, Digital Micromirror Device(DMD), Interferometer and Camera Unit. Several laser diodes emit a laser beam that is coupled in an optical fiber and projected on the DMD which modulates the beam and transfers a pattern corresponding to the pixels in an image onto resist coated substrate.
A Digital Micromirror Device for spatial light modulation of laser light is used to project and transfer a pattern onto a resist coated substrate.The Camera Unit has one low resolution, one high resolution and one overview camera that are used for accurate alignment of a design with existing structures on a substrate. The laser interferometer is used for measuring stage position.
The data entered by the user is processed by the components located in the Electronics Rack.
The Stage Controller drives the stage through linear motors in both axes, the movement is controlled based on feedback from interferometers in the main unit which triggers the laser and DMD.

2. FABRICATION STEPS

2.1 MASK LAYOUT

A) DOSE/DEFOCUS MATRIX

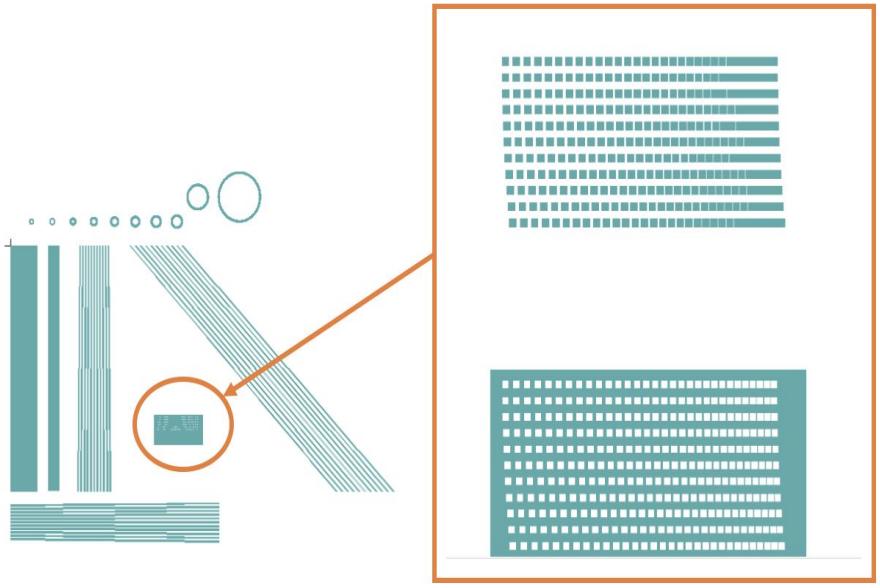

Figure 2: Dose/ Defocus Mask Layout

1) Ridge Matrix

Arrays of 5 μm × 5 μm squares with decreasing spacing (3 to 0.1 μm) shifted by 0.1 μm in each row.

2) Trench Matrix

Inverse of Ridge Matrix such that the spacing between the boxes is the part that gets exposed.

B) TIME/ TEMPERATURE REFLOW MATRIX

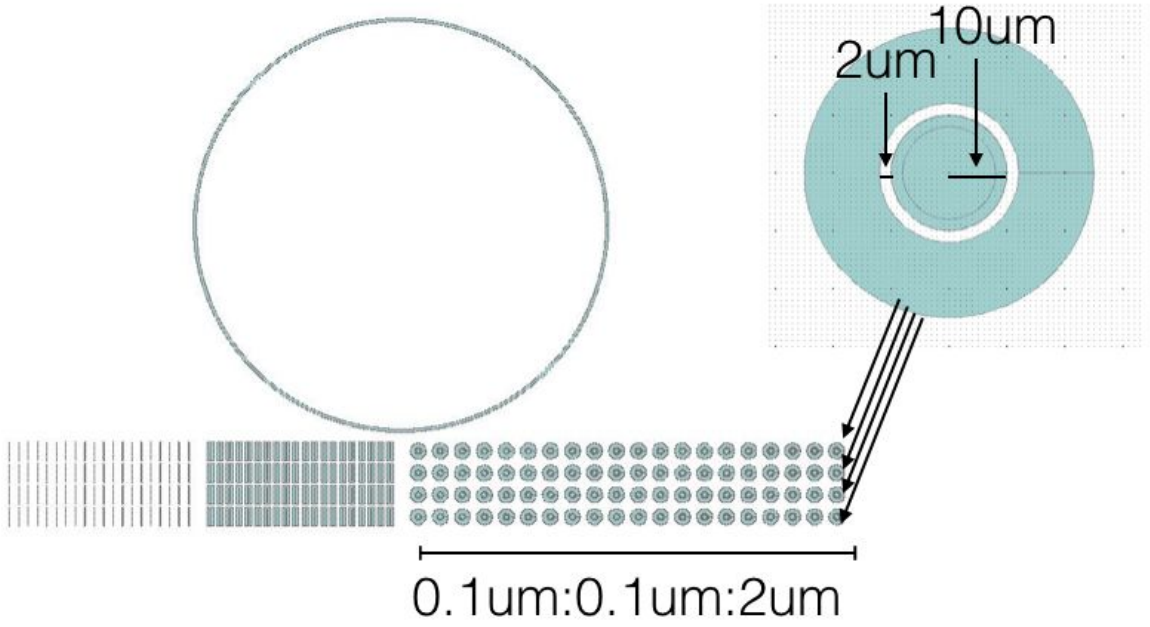

Fig 3: Time/ Temperature Matrix Mask Layout

1) Ring Matrix
   - x4 identical arrays of PR rings with increasing ring width, going from 0.1um wide to 2um wide
   - Inner radius = 10um

2.1 PROCESS FLOW

1. Standard Piranha Clean of 4" L Prime Wafer.
2. Waveguide Stack Growth : 450 nm of silicon nitride on 2.85 µm of silicon oxide.
3. Singe and Prime wafer
   Using YES Oven. This process dehydrates the wafer at 150°C and primes the wafers using HMDS (Hexamethyldisilazane) which increases adhesion between oxide and resist.
4. Spin coat resist on wafer
   This is done using SVG Resist Coat Tracks 1&2. We use Shipley 3612 Photoresist with a thickness of 1 µm and 2 mm Edge Bead Removal.

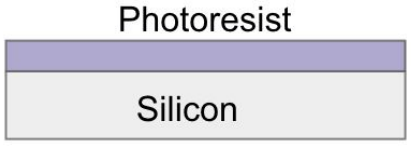

Figure 4: Resist on wafer

5. Perform exposure using Heidelberg

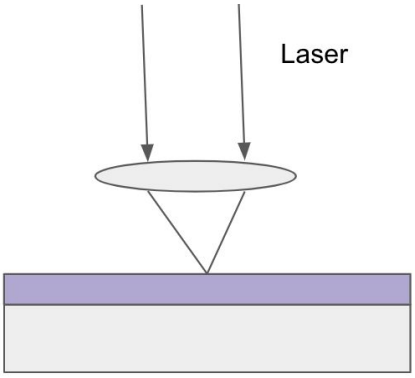

Figure 5: Maskless Lithography Step

- Create a dose/ defocus matrix of the pattern on the wafer using Mask Layout No.1
- The dose varies from 91 to 60 mJ/ cm^2 , and defocus from -5 to 4 which gives us a 32×10 matrix.

6. Develop the pattern

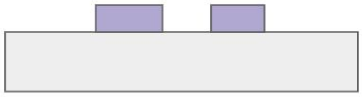

Figure 6: Developed pattern on wafer

This is done using the SVG Develop Tracks 1&2.

7. Image all Ridge and Trench Matrices using optical microscope

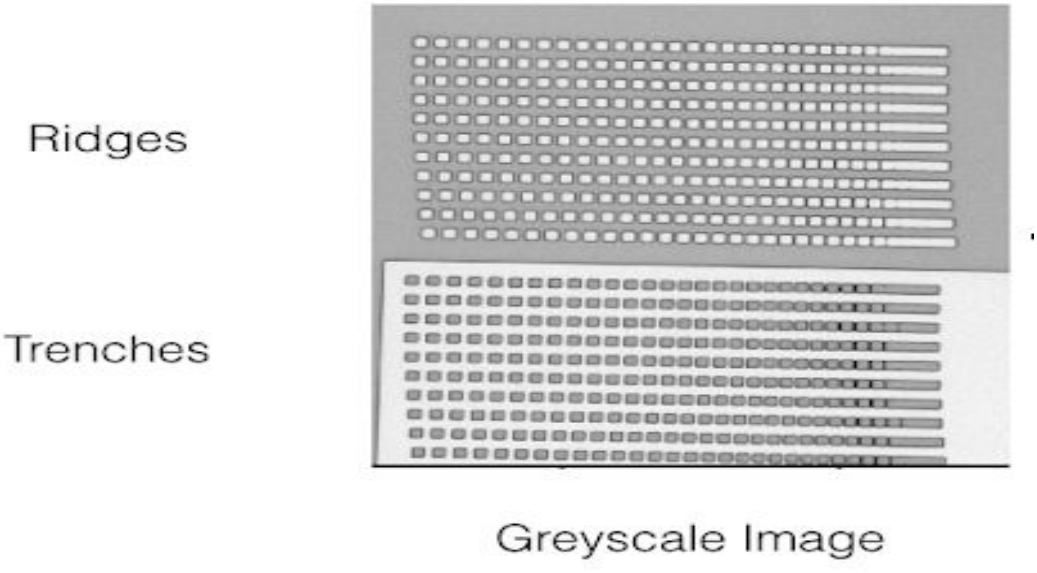

Figure 7: Optical image of ridge + trench matrix

8. Determine optimum Dose/Defocus
    a. Explained in section 5.

9. Repeat above steps to fabricate wafers on which thermal reflow of Photoresist will be conducted using the optimum Dose/Defocus obtained in Step 8 using Mask Layout No.2

10. Laser dice the wafers obtained to create individual chips.
    a. Explained in section 5.
11. Conduct Photoresist Thermal Reflow using different times and temperatures on different chips
    a. explained in section 4.

12. NOVA SEM Reflowed dies
    a. Cressington Sputter: 5nm
    b. NOVA SEM
        i. Immersion mode images of rings fabricate using Mask Layout # 2
13. Obtain best time temperature
    a. Explained in section 4

14. Etch Steps
    a. Use Silicon Nitride test wafer, do a 30 second etch
    b. With nanospec measure and calculate thickness change of test wafer
    c. calculate etch rate
    d. Use nanospec to measure etch distance
    e. Calculate time for a 30% over-etch (standard)
    f. Attach die to carrier pocket wafer and run
15. PR removal
    a. Attach die to carrier pocket wafer
    b. Recipe: 013
16. AFM characterization of sidewall profile for waveguides etched for with and without PR reflow.

3. IMAGE ANALYSIS SOFTWARE

3.1 DOSE/DEFOCUS MATRIX ANALYSIS

An important limitation of the Heidelberg as compared to the ASML or e-beam lithography tools is the resolution. According to the SNF website, a resolution of 1 micron is quoted. For this project, we set out to characterize and optimize the minimum features we could resolve based on dose and defocus for 3612 1um Shipley photoresist on standard 4’ silicon wafers (L-prime) and on our waveguide material stack which consists of 450 nm of silicon nitride on 2.85 μm of silicon oxide.

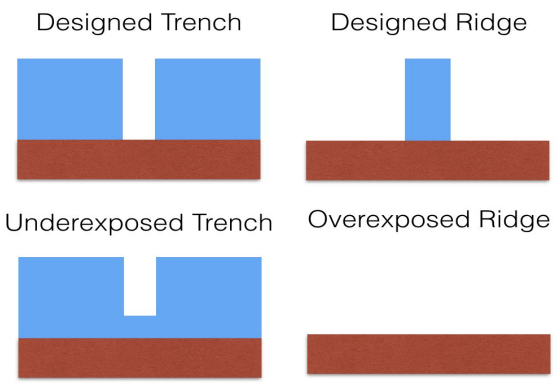

Figure 8: Example showing effect of over/under exposure on the patterned trench and ridge

We choose to use two metrics for resolution: minimum ridge width and minimum trench width. Our suspicion was that high doses improve the resolution of trenches. Low doses improve the resolution of ridges. Too high of a dose would destroy thin ridges, while too low of a dose would underexpose trenches as shown in Figure 4.1. Improving the defocus (which roughly corresponds to focal depth [1]) would improve both the ridge and trench resolution.

In order to test this, we used the above design to create a dose defocus matrix from 60 mJ/ cm^2 to 91 mJ/ cm^2 , and our defocus went from -5 to 4.
Using the optical microscope in the SNSF, we took pictures at x20 mag over the entire dose defocus matrix. One image for the pits/ridges (top) and one image for the boxes/trenches (bottom). These images were then fed into a software program that extracted the number of resolvable boxes or inverted boxes, which we refer to as pits (seen below). Due to over or under exposure, there would be a difference between the number of designed boxes or pits and the exposed boxes or pits along a single layer. Since boxes or pits were separated by increasing increments of 100 nm, an effective resolvable width can be calculated based on this difference in box/pit number.

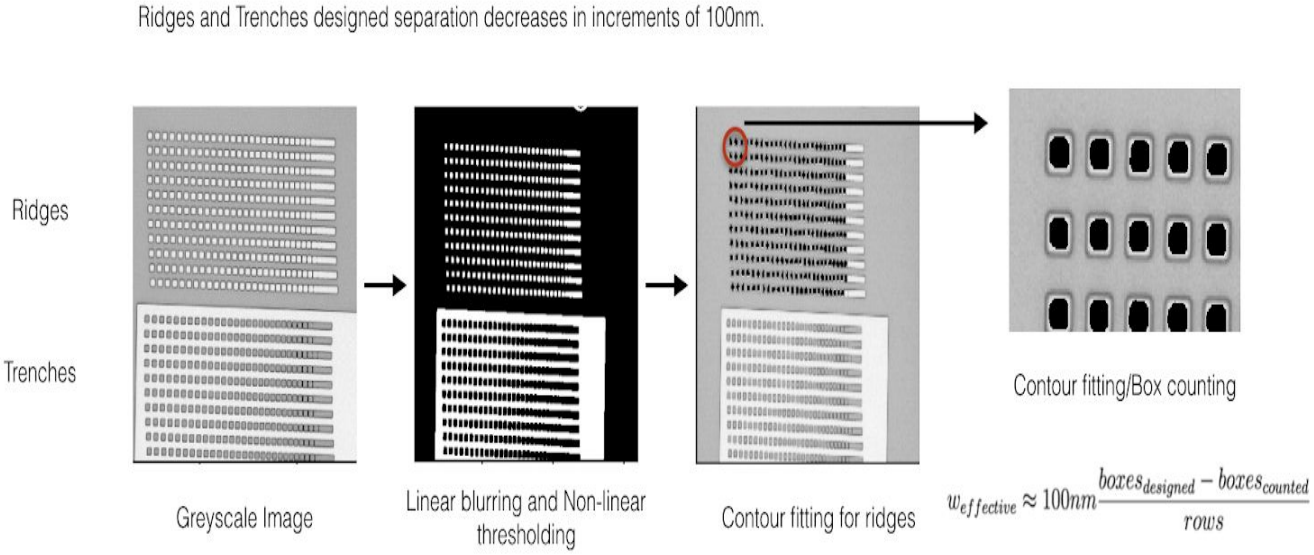

Figure 9: Image Processing steps for Dose/Defocus Matrix Analysis

$$w_{effective} \approx 100nm \frac{boxes_{designed} - boxes_{counted}}{rows} \quad (4)$$

The minimum effective trench width and ridge width show three trends. First, lower defocus improves resolution for both trenches and ridges for our silicon photoresist stack. Secondly, smaller dose improves the resolution of ridges, while reducing the resolution of trenches. Thirdly, larger dose improves the resolution of trenches, while reducing the resolution of ridges.It seems then for dose there exists a tradeoff between minimum resolvable trench and ridge dimensions. We took the above data tables, and applied a squared sum score with an alpha weighted towards ridges to choose the best dose/defocus pair. Larger alpha values correspond to better ridge resolution while smaller alpha corresponds to better trench resolution.

$$score = \alpha(w_{ridge_{eff}})^2 + (1-\alpha)(w_{trench_{eff}})^2 \quad (5)$$

Since for most users over-exposure is preferable to under-exposure, and trench resolution is more important, we chose an alpha of 0.2.
Result: Best Dose Defocus for Resist on Silicon: (80,-5)
Result: Best Dose Defocus for Resist on Waveguide Stack: (80,-3)

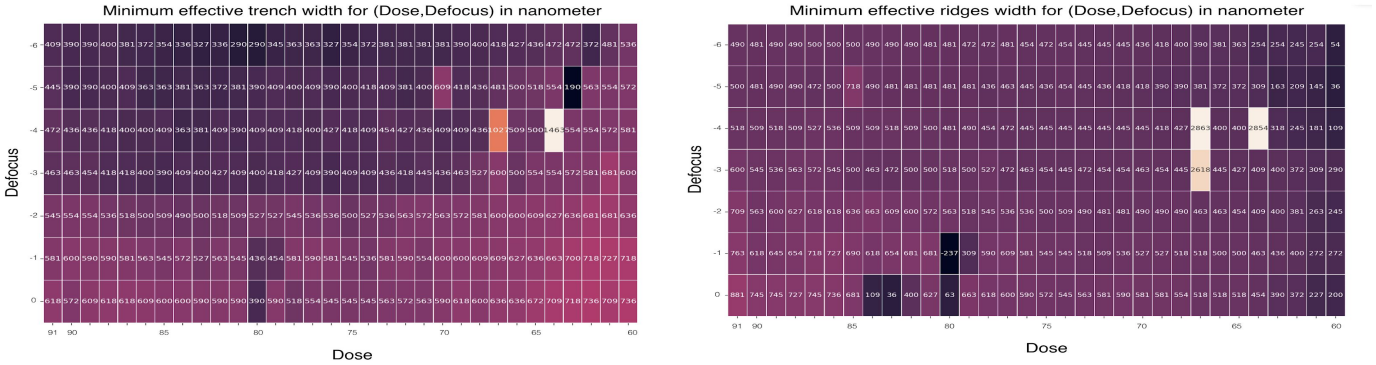

Figure 10: Data obtained from Software to extract Minimum effective Trench and Ridge width across Dose/Defocus Matrix for Photoresist on Silicon

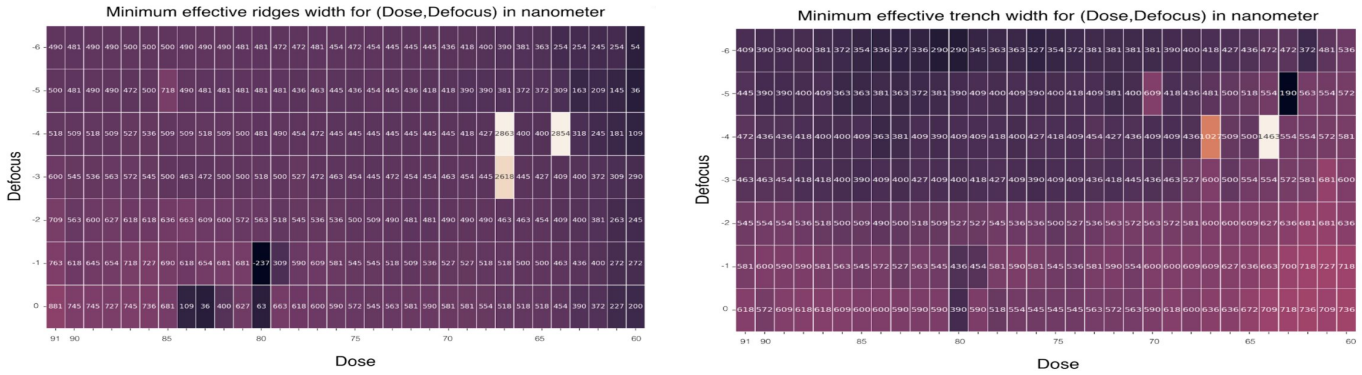

Figure 11: Data obtained from Software to extract Minimum effective Trench and Ridge width across Dose/Defocus Matrix for Photoresist on 450nm LPCVD Stoichiometric Silicon Nitride on 2850 nm Thermal Oxide

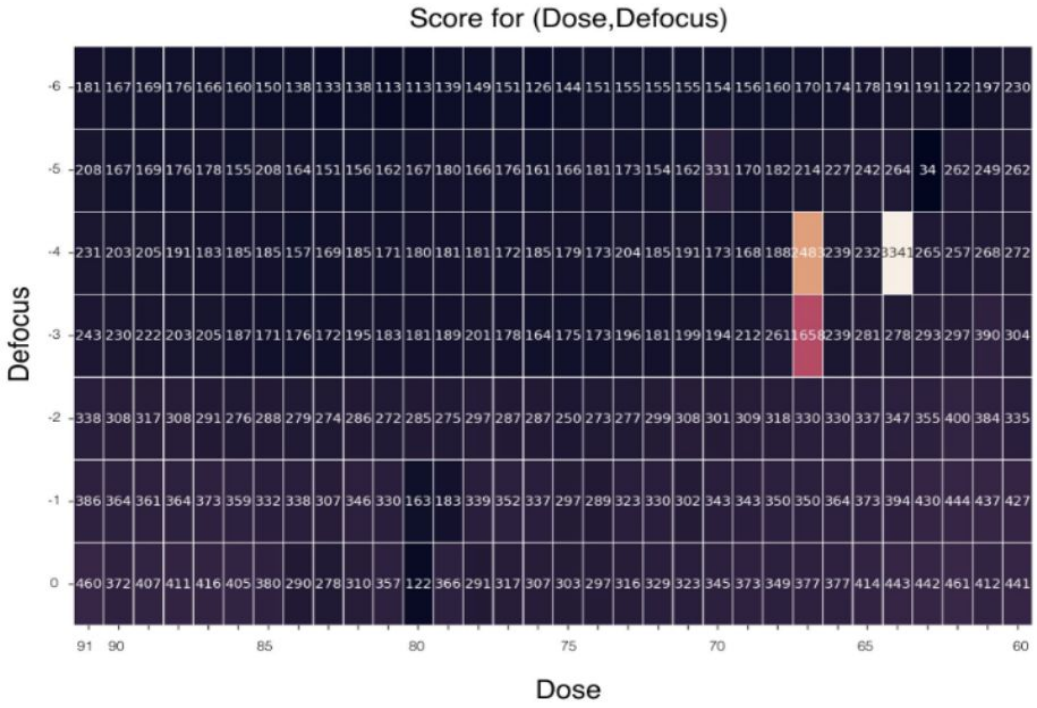

Figure 12: Calculated Score for Dose/Defocus Matrix for Photoresist on Silicon. The high scores around -4 defocus, 65 dose, correspond to large scratches transferred during fabrication.

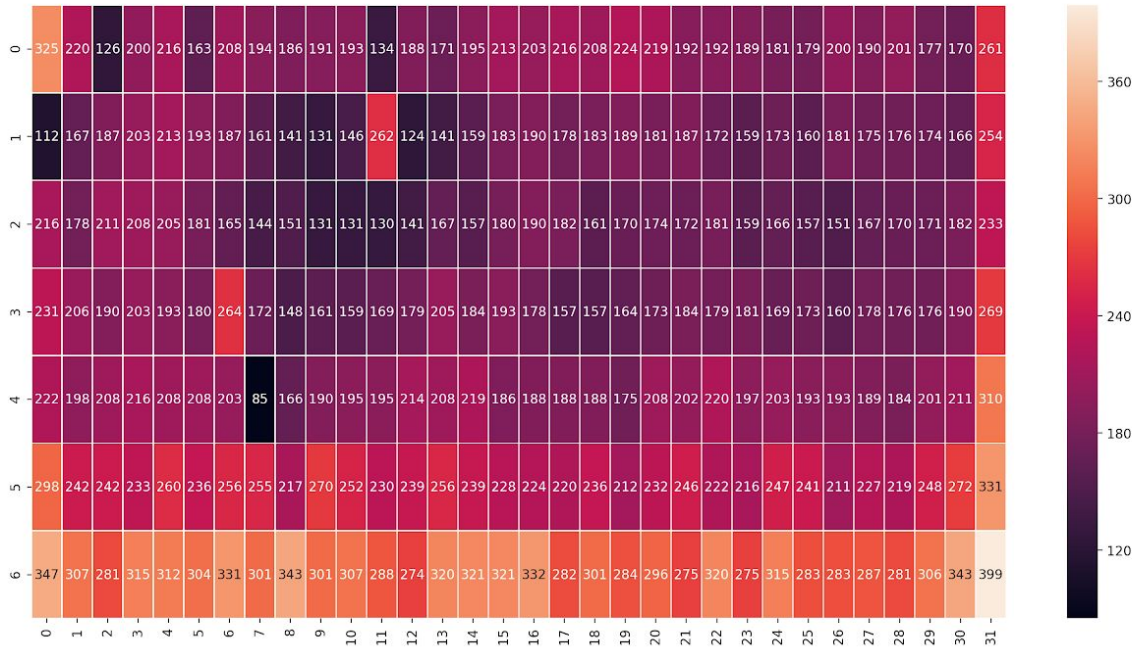

Figure 13: Calculated Score for Dose/Defocus Matrix for Photoresist on 450nm LPCVD Stoichiometric Silicon Nitride on 2850 nm Thermal Oxide

3.2 LINE EDGE ROUGHNESS EXTRACTION

Overview

A known issue with the Heidelberg comes from transfering long straight lines that are angled. To characterize this problem, we exposed long angled ridges and then took high resolution SEM images of individual sections. Using stitching software, we reconstructed long sections and did image analysis to extract the line profile. From this line profile we did LER and LWR analysis.

Important Note

No clearly observable low frequency LWR or LER was observed on waveguides printed on Manhattan grid. ***The solution to removing angled line LER and LWR is to not use angled lines.***

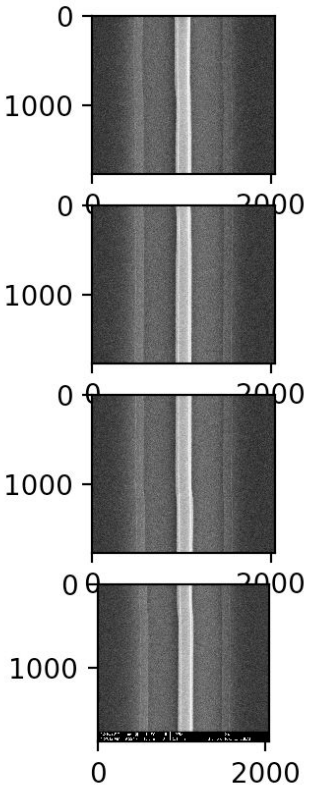

Figure 14: Multiple NOVA SEM images of a 1mm long, 0.5°, 1.6um PR strip on Si.

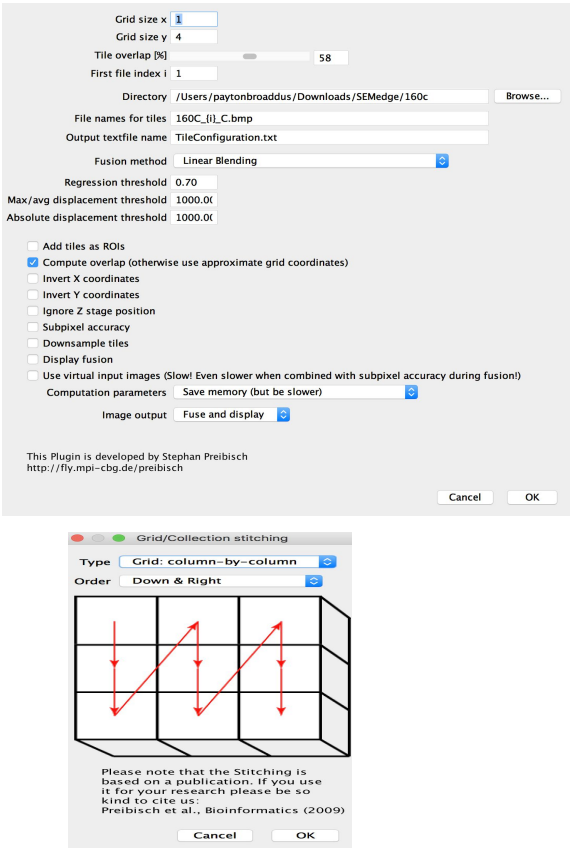

Figure 15: Fusion method and parameters used for stitching images.

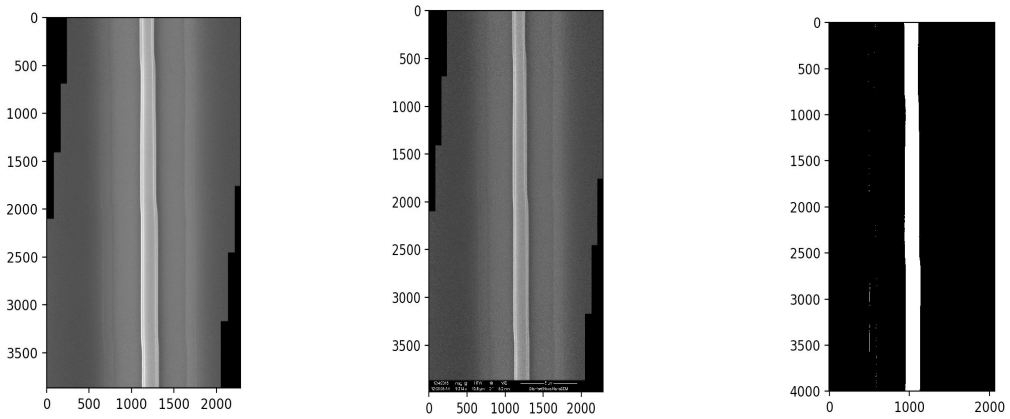

(A) (B) (C)

Figure 16: (A) Stitched image without legend (B) Stitched image with legend (C) After edge detection

Image processing to get line edge roughness and line width roughness

We take the images stitched together and extract the curves in Python script using OpenCV. This is done in the following order:
Gaussian Blurring ⇒ Thresholding ⇒ Morphological opening (Denoising) and Closing (remove holes) ⇒ Erosion ⇒ Morphological Opening ⇒ Multiple steps of Blurring and Thresholding.
Finally a Canny Edge Detection Algorithm is used to find the two edges of the PR ridge.

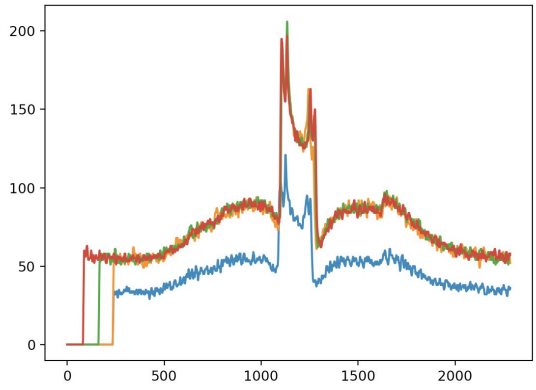

Figure 17: Grayscale values of SEM images of transverse profile of angled photoresist ridge.

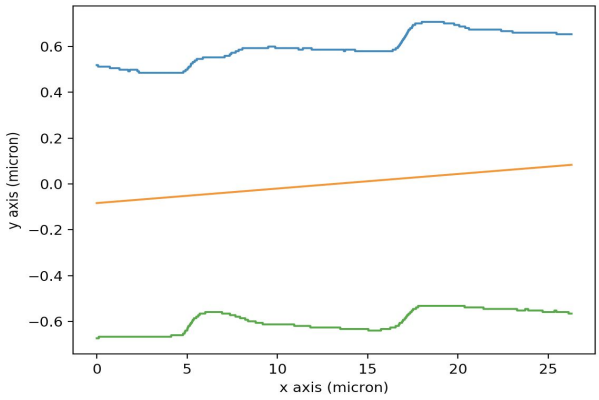

. Figure 18: Transverse Profile of waveguides at different positions where Green and Blue: Edge profile, Orange: center angled fit

Finally, we extract the edge profile. Units of length are taken from the scale bar, and used to map the curves to relative positions. Above a line representing the original midpoint is generated.
Designed angle: 0.57 degrees
Measured angle: 0.40 degrees
Furthermore, we used a simple RMS calculation to described the LWR and LER.

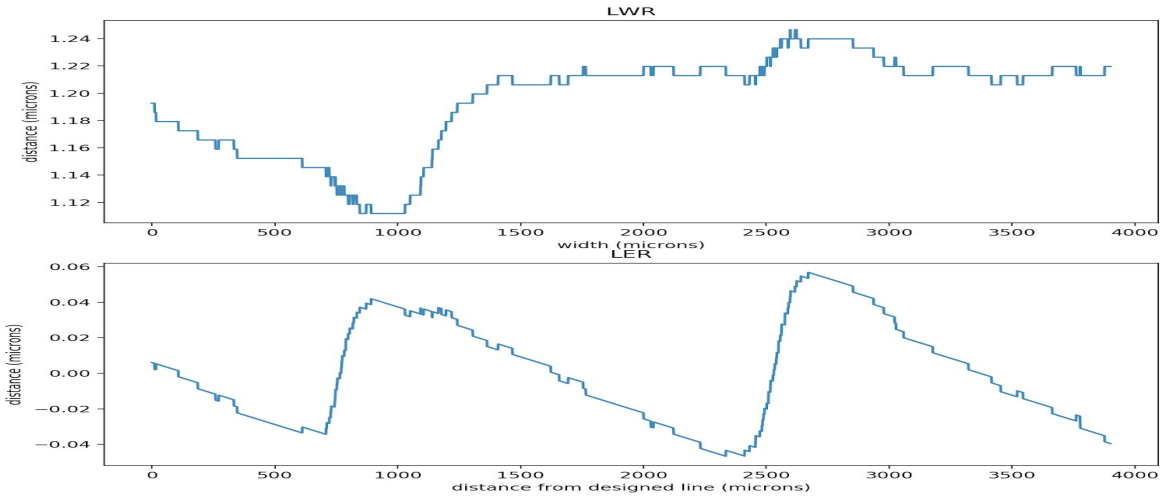

Figure 19: LWR and LER roughness of 0.5 ° tilt 1.6um lines

LWR: 0.0353 um
LER: 0.0285 um
SEM Pixel resolution: 0.0067 um
The FFT analysis (not shown) doesn't capture that most LWR comes from large frequency swings. This is due to large noise at low spatial frequency. Code is provided: https://github.com/broaddus/HDW

4. TIME/TEMPERATURE EFFECTS ON PHOTORESIST REFLOW

4.1 METHOD

The wafer patterned with Mask Layout 2 is diced using the Laser Dicing method in Section 5. To study the effect of time and temperature on photoresist roughness and its lateral spreading, the chips are heated on a polished and cleaned aluminum slab placed on a programmable hotplate. This is done to keep the process clean for further etch steps.The hotplate temperature is calibrated with a metal thermometer.

(4, 140)	**(4, 140)**	**(4, 160)**	**(4, 170)**	**(4, 180)**
(5, 140)	**(5, 150)**	**(5, 160)**	**(5, 170)**	**(5, 180)**
(6, 140)	**(6, 150)**	**(6, 160)**	**(6, 170)**	**(6, 180)**
(7, 140)	**(7, 150)**	**(7, 160)**	**(7, 170)**	**(7, 180)**
(8, 140)	**(8, 150)**	**(8, 160)**	**(8, 170)**	**(8, 180)**

Figure 20: [Time(minutes), Temperature(℃)] Matrix of conditions used for reflow

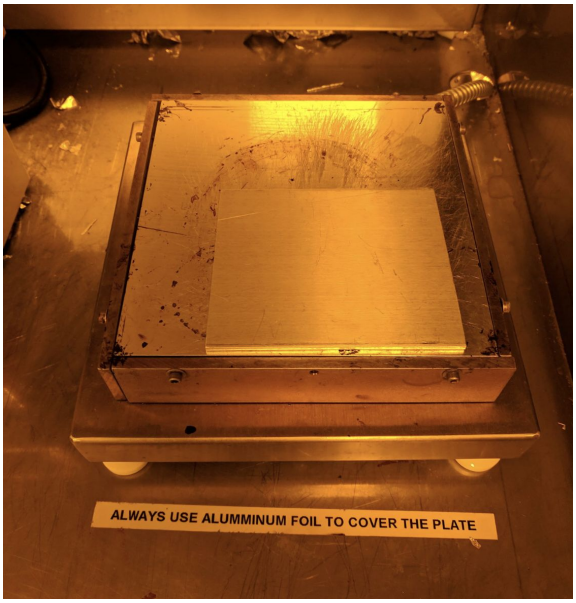

Figure 21: Polished aluminum slab placed on hotplate used for carrying out reflow.

The aluminum slab was cut and polished in the Stanford Physics Machine Shop. The plate then underwent degreasing wash with Acetone, Methanol and Isopropyl Alcohol, in the same order followed by a 5 minute DI water rinse.

4.2 KEYENCE CHARACTERIZATION

Initially, to characterize the LER and LWR of the photoresist rings, we used the Keyence Microscope in the SNL. However, the resolution, approx. 100 nm/pixel, was not high enough to resolve the low frequency components of the LER. The LER of the PR rings we measured with this tool was only slightly larger. However, Keyence measurements of these rings were still useful, since the 100 nm noise floor set an effective upper limit on the LER of these rings.

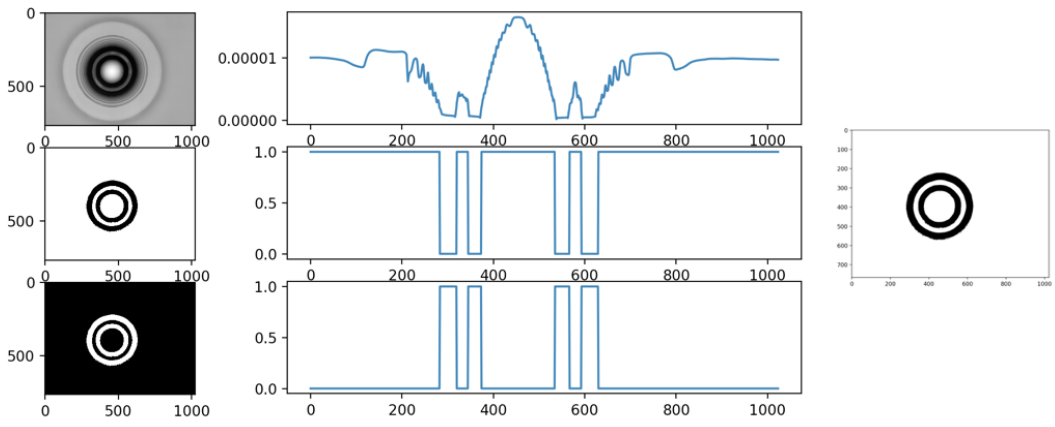

Figure 22: Data obtained from Keyence Microscope

4.3 NOVA SEM CHARACTERIZATION

We achieved an order of magnitude better resolution, ~10 nm/pixel, with the NOVA SEM in the SNL. High resolution, 30μm wide images of the rings were taken. Contrast and brightness settings were chosen individually for each Time Temperature set of rings, but among a single Time Temperature ring array were constant. Immersion mode was required in order to get the profiles. The data was saved as a bmp file.

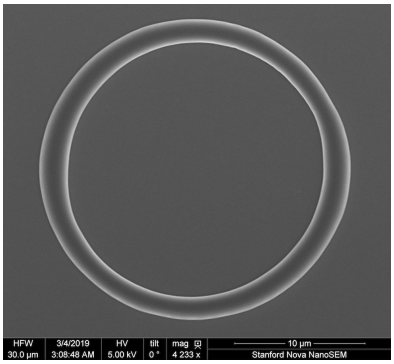

Figure 23: Image of reflowed ring(5min, 180°C), initial width of 1 μm.

4.4 LER and LWR CALCULATION

These rings were then fed into a software program that extracted the profiles of the inner and outer edge of the rings. This software was built using an edge detection algorithm developed in the previous quarter. Good edge detection and extraction requires good initial contrast on the waveguide edges relative to the substrate underneath. The extraction followed a similar pattern to the dose defocus extraction, but was much simpler due to better signal (ring edge) to background (substrate) contrast.

Initial software process flow: Remove legend -> Gaussian blurring -> Calculate median greyscale value -> Binary threshold (median+5) -> Canny edge detection -> Filter edges (based on area and perimeter) -> outer and inner edges correspond to ring edges

Sometimes the data were very noise or the greyscale contrasts were not good. In that case we would:

a) Retake SEMs with fresh Au/Pd alloy coating
b) Use an adaptive filter and save binary threshold image
c) Fix the gaps in the ring of the saved binary threshold image with ImageJ
d) Rerun software with fixed binary images
e) If the “gaps” were too large (more than a couple pixels), that data would be thrown away

Once the edges were identified, the coordinates of the individual points of the profile were averaged to find the center (this minimizes mean square error of circle fit). The center was subtracted from all data to place the points around the origin, and a polar transform was done to “unwrap” the edge profiles. A linear interpolation was done on both data to allow a one to one comparison of the inner and outer ring profile. The LER of the inner and outer unwrap edge profiles were calculated, using nm/pixel data calculated from image dimensions (pixel) and image width (nm), as well as the LWR of the difference between interpolated data. Another key data point was the new width: the difference between average radius of inner and outer profile. The LER and LWR was clearly visible in the “unwrap” profile, and the LER and

LWR calculated was 5+ times larger than the discretization error (~10nm/pixel), giving us confidence we had accurately measured the LER and LWR. The program flow of one ring image is shown below.

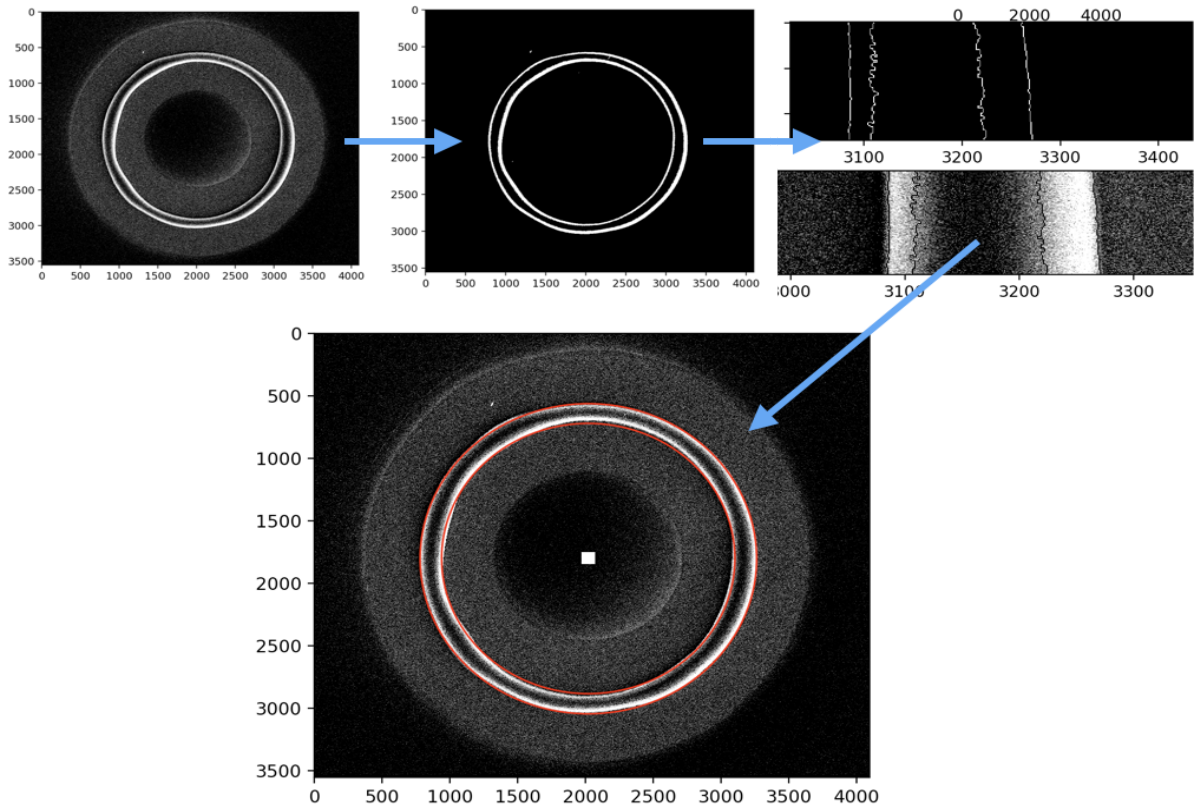

Figure 24: Edge detection applied to photoresist rings.

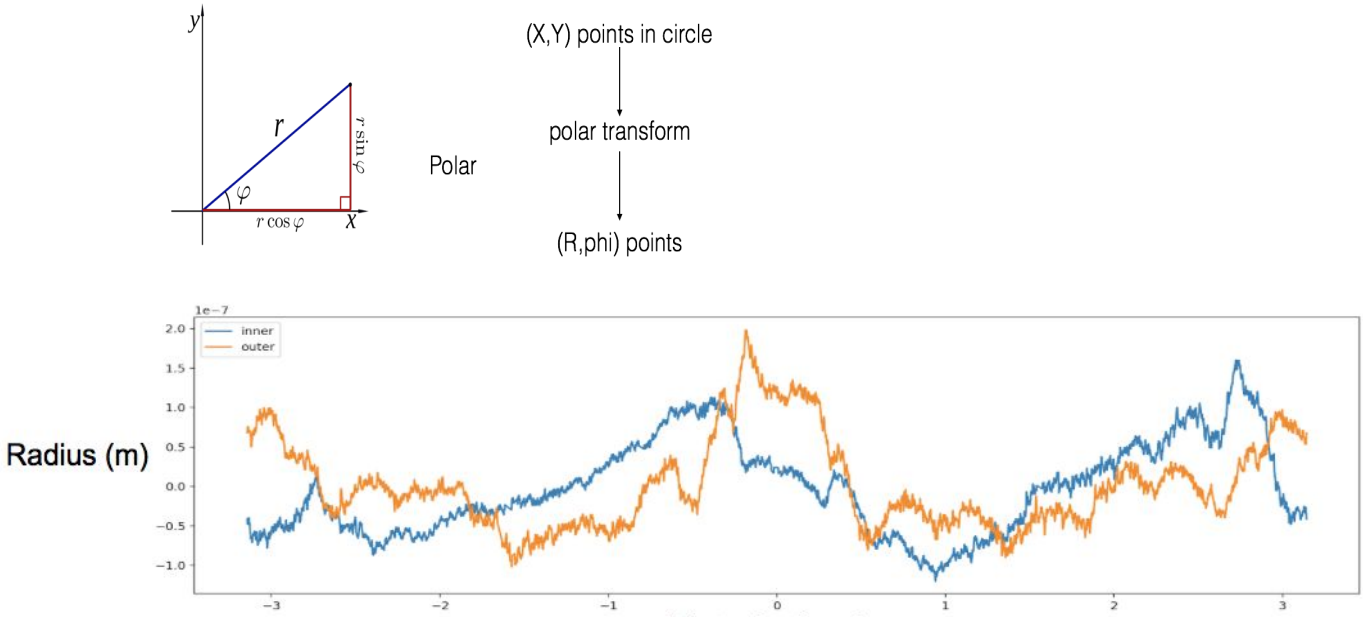

Figure 25: Unwrapped mean zero inner and outer edge of a ring. Notice the theta spans 2π, since it is a circle.

4.5 RESULTS FOR LWR AFTER PHOTORESIST REFLOW

The profile data for each time and temperature, as well as a reference (no reflow), were calculated. Two data points were extracted for each ring width for each time,temperature: the width of the ring after reflow and the LWR of the ring after reflow. Below the results were plotted for each temperature and time, the LWR of the ring vs the width of the ring (after reflow)

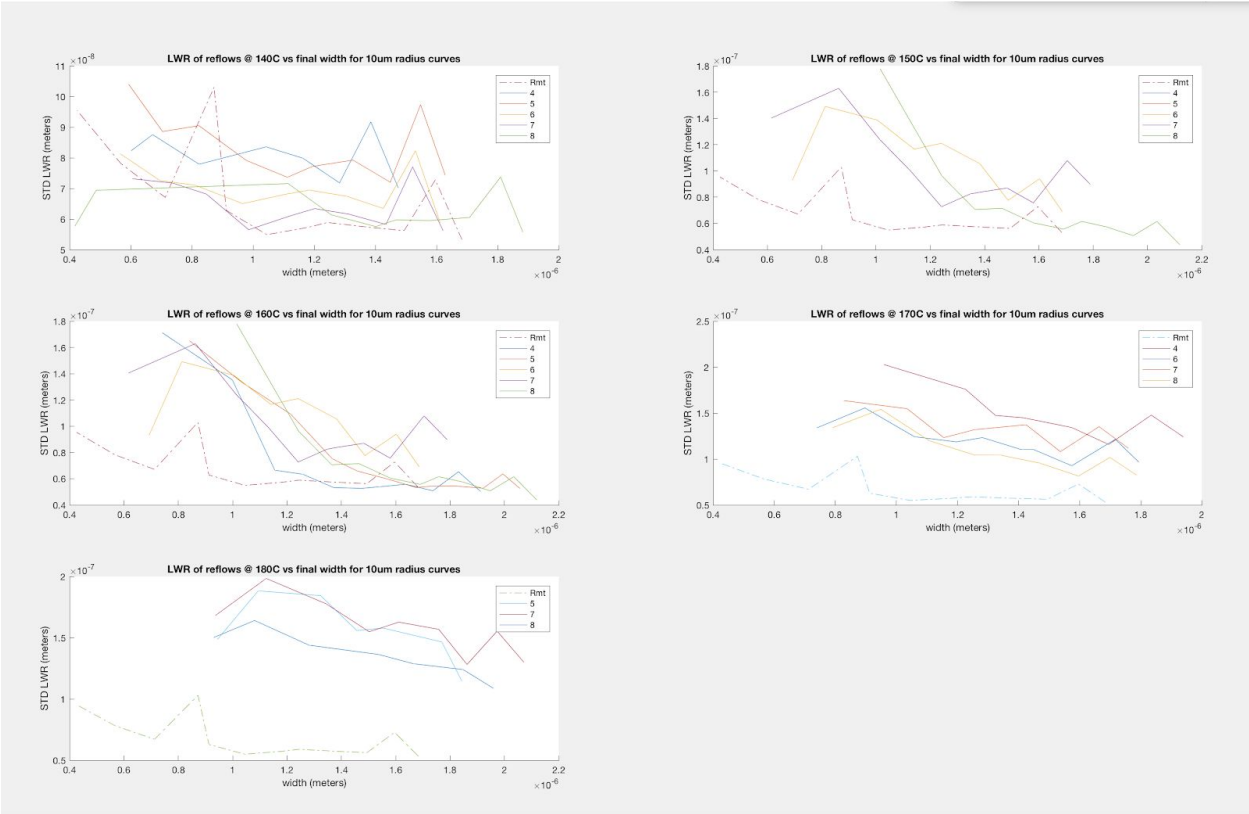

Figure 26: Plots of LWR versus photoresist width for various times at different reflow temperatures.

As seen above, high temperatures (180C,170C) increased both the width of the ring as well as substantially increase the LWR. This makes high temperature reflow counterproductive for waveguides. This trend is seen with 160C and 150C, although the growth of width and LWR is decreased. At 140C, the width doesn't increase until 8 minute mark, at which point the width increases. At all times for 140C, the LER stays constant. This implies low temperature long time reflows could be useful for changing ring widths post-develope, although another possible explanation is that low temperature long time reflows are still increasing LER, just below the SEM noise floor.

Although we were hoping in seeing a reduction of LER at some temperature, our data shows that reflow potentially could be used to change the resolution of features post-develop, by slowing increasing width of rings or other ridges. More useful, though, would be decreasing the widths of trenches in PR, enabling sub-lithographic-resolution limited trenches to be defined and subsequently etched.
These data, as well as the code to generate it, is available here: https://github.com/broaddus/HD

4.5 WAVEGUIDE PROFILE AFTER ETCHING

To test the etch characteristics of reflowed rings, two dies, one reflowed at 140C for 8min and one unreflowed, were attached to carrier pocket wafers, and etched with the standard Chamber B Ox recipe, and afterwards, on a seperate pocket wafer, the PR was removed with gasonic 013 recipe. To look at sidewall steepness, as well as get an accurate width of ring, we took these dies to the XE-70 AFM. Both reflow and unreflowed showed similarly steep profiles (good for waveguides), with the reflowed showing a width increase of 400 nm. Shown below is the AFM data of 2 μm width rings.

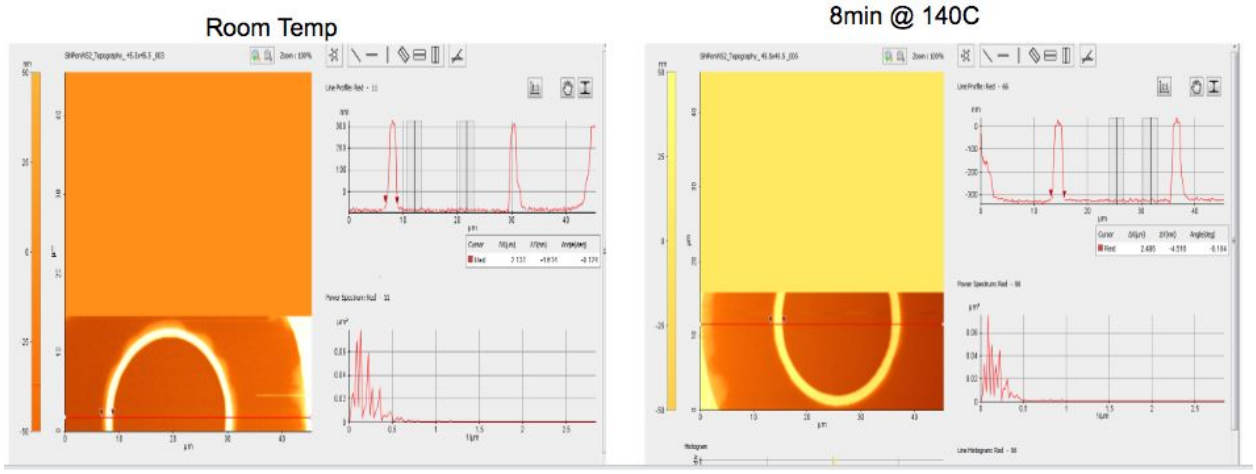

Figure 27: Profile of etched rings for no reflow and for the optimum time/ temperature condition.

5. LASER SCRIBING AND DICING

5.1 OVERVIEW

Unique to our project was the need to dice a wafer for reflow studies without doing a cleaning step that would remove the photoresist pattern. There are a number of PROMs and SOPs for dicing wafers and moving those dies back from contaminated group to clean group, allowing use in clean tools. However, these steps involve coating the wafer with thick protective photoresist layers and harsh wet chemical cleans (to remove protective photoresist layer).
In order to generate lots of clean dies with PR patterns, we needed a way to either pattern a number of cleaned dies quickly or do a clean dicing step without removing any surface PR. One such tool that could potentially do very clean dicing was the Lasercutter in exFab.
However, no SOP existed for using this tool or dicing wafers. So our project completed two objectives: Make a SOP for using the Lasercutter to scribe/dice wafers, and building a clean Wafer holder such that the wafer surface does not get contaminated.

5.2 WAFER-HOLDER FABRICATION

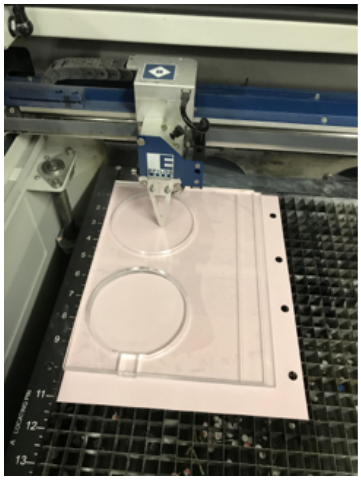

Figure 28: Our acrylic wafer-holder

Figure 29: Laser scribed test wafer

We designed, lasercut, and assembled two acrylic wafer holders with acrylic cement. These wafer-holders then underwent a 5 minute water wash at a flexcore bench. One wafer-holder is dedicated to clean cutting (no metal groups). The wafer-holder contains a recess where a wafer can lie, and the (0,0) mark of a laser cut file corresponds to the center of the circle the wafer. This allows accurate general drawing.
Alignment Accuracy: ~1mm.

5.3 LASERCUTTER SOP

We wrote a turnkey guide to using the Lasercutter. This includes a laser-scribing guide, laser-dicing guide, and includes general laser cutter tips and tricks as well as general measurements for cut width and alignment accuracy.

5.4 PROCEDURE

A wafer is loaded front face down inside the larger recess on the wafer-holder. A small acrylic stop piece is used to hold the wafer in place. The laser is then put at focus using the offset with the second recess (explained in SOP). Using a standard template laser cutter file (such as 10mmx10mm), and using laser and file parameters defined in the SOP, the laser scribes the back of the wafer. Using a clean wafer cleave plier, manually dice the wafer.
Afterwards, in a clean container, take the dies back to the main lab and do a thorough 5 minutes wafer clean. The dies are now conditionally in the clean group, without removing or damaging PR on the front. This entire process flow is explained in the PROM section of the SNF website.

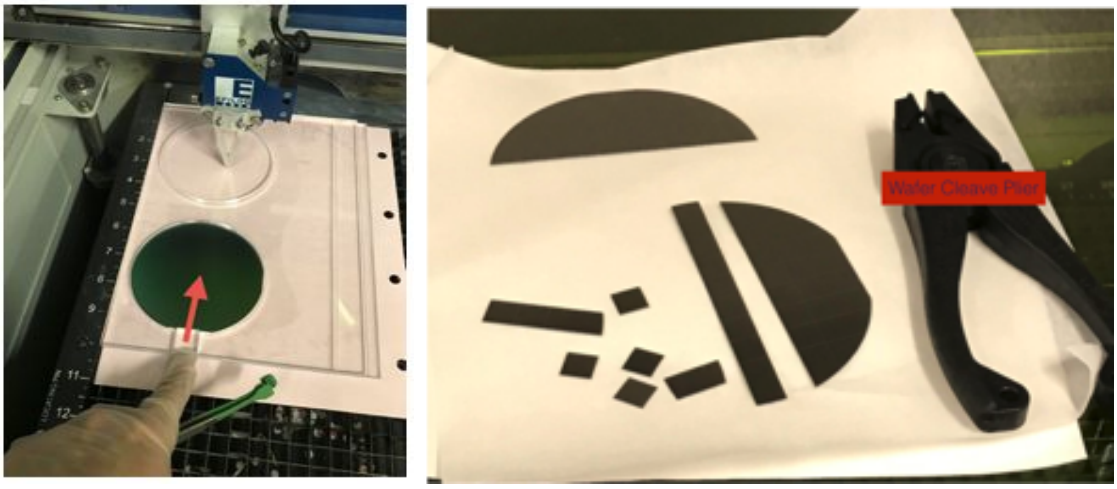

Figure 30: Wafer placed upside down on wafer holder for scribing and chips obtained with wafer scribe pliers.

The SOP includes also standard laser settings for dicing different materials, with a table on the back for users to add to.

6. WAVEGUIDE TESTING

6.1 OVERVIEW

We first developed straight silicon nitride waveguides with the Heidelberg and characterized its loss. Without reflow, we defined and etched stoichiometric silicon nitride dimensions of ~450 nm x 1.6um on 2850nm of BOX (Buried Oxide). Afterwards we used PECVD system (ccp-dep) to deposit a 1.5um of oxide capping layer. The wafers were then scribed with the laser cutter and diced with a wafer cleave plier, producing dies 5mm width by 29mm long, each with an array of waveguides, each waveguide separated by 100um. These dies were then sandwiched between two glass dies of similar size, loaded on a CMP and double polished overnight. Finally, these waveguides were loading into a optical setup designed to measure loss.

6.2 POLISHING

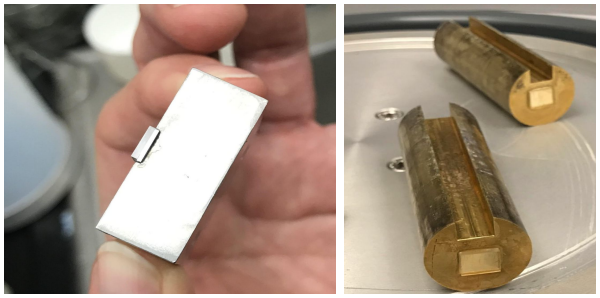

Figure 31: Polished edge and two brass polishing holders

The dies are were loaded five at a time in each brass polishing holder, shown below. This stack of dies was sandwiched between two glass dies of similar dimension, all held together in the brass holder with Crystalbond™. A two step polish process was used: First a short polish with a 10 μm grit slurry was used, followed by a long 5-10 nm grit slurry polish overnight. This two step polish was then repeated on the other edges. Afterwards, the facets were inspected with a x150 microscope.

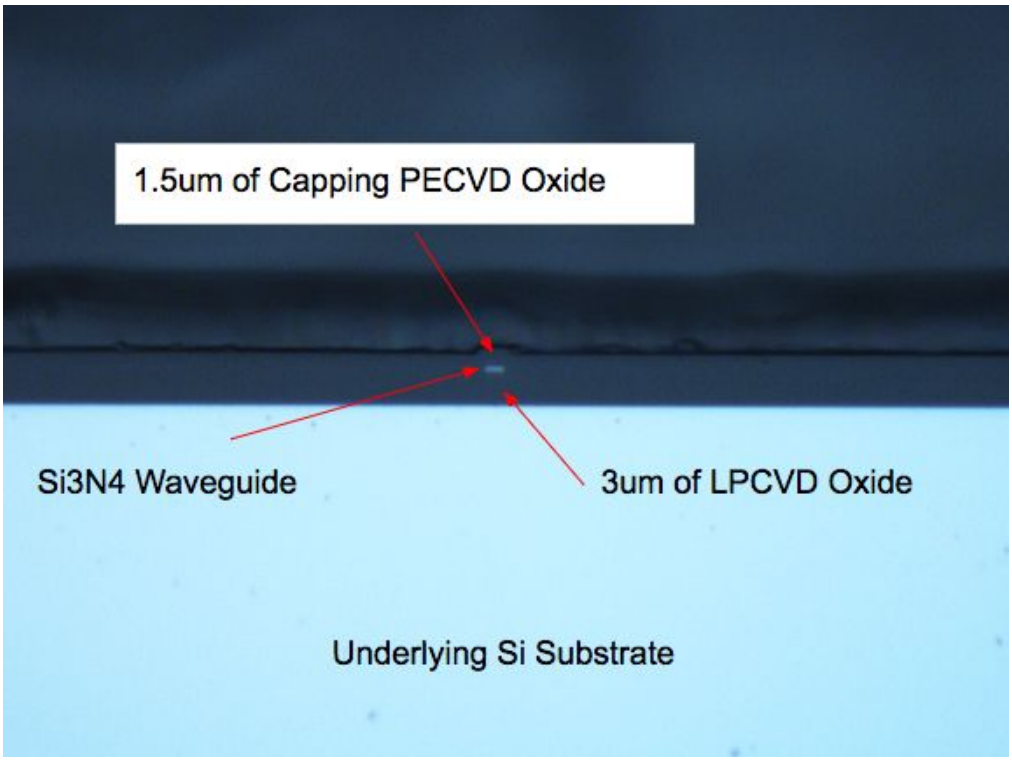

Figure 32: Cross-section of polished silicon nitride waveguide with capping oxide.

Note: Most groups will want to use the Ginzton Crystal Shop shop to polish. The lab manager, Tim Brand, can be contacted here: tbrand@stanford.edu

6.3 COUPLING IN LIGHT

We used a 1.55um fiber laser coupled into input/output f=4.8mm lens for all loss measurements. This entire optical setup fed into either an InGaAs camera for alignment or a Ge photodetector for loss measurement. Initially, only a input f=5mm lens (no output lens) was used for easier alignment, followed by a progressively smaller focus output and input lenses.
The waveguides we produced are highly confined modes, lower index contrast or larger core waveguides will result in large mode areas and easier coupling. In fact, while aligning, the camera detector showed diffraction rings around the central mode. These rings are not fundamental to the mode, they came from the lenses themselves acting as apertures. Issues like this can be solved with higher NA lenses. Edge coupling light into a waveguide is difficult.

Figure 33(above,left): No output lens, looking to maximize rate of change of diffraction pattern vs Z sweep to find top edge die.

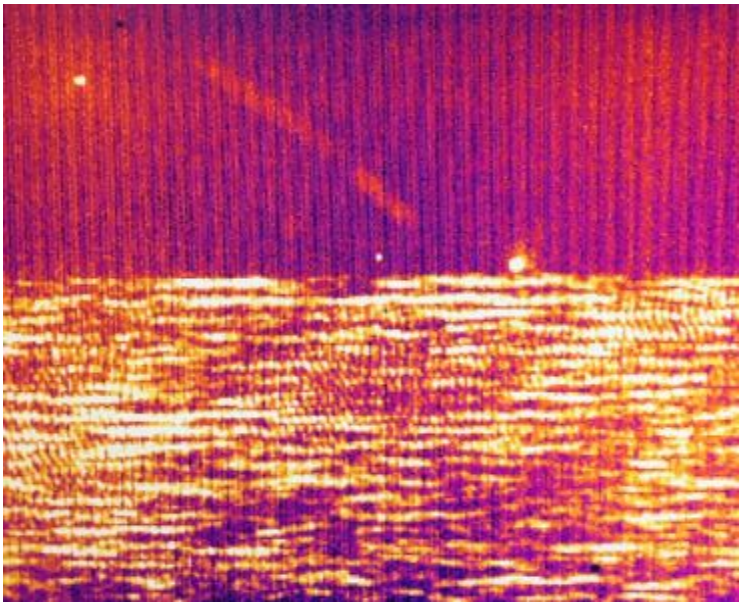

Figure 34: w/ focus output lens, notice waveguide mode output above oxide in center right of image

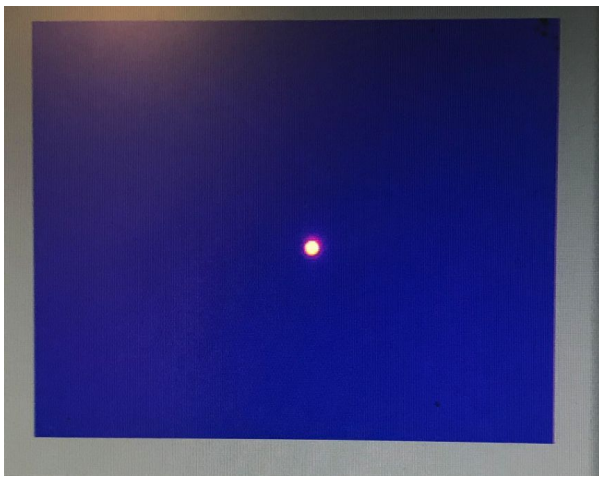

Figure 35: Well aligned lens system with wave-guide output.

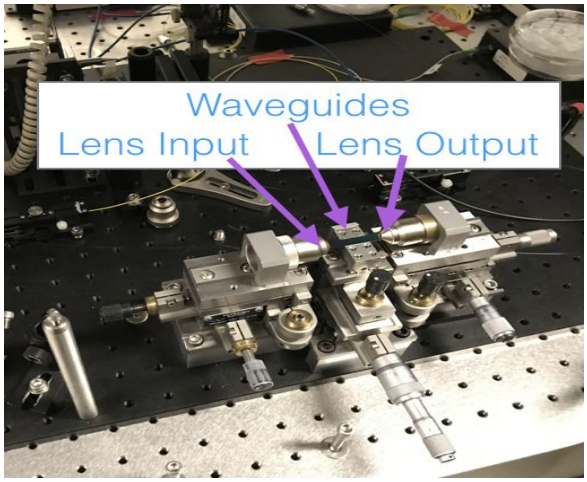

Figure 36: Optical setup for measurements.

6.4 LOSS DATA

Each die contained an array of waveguides, each separated by 100um. Since the waveguides are all aligned and on same plane, coupling into one waveguide massively simplifies coupling into the others, since moving the stage left or right 100um re-matches the waveguide mode and laser mode nearly

perfectly, requiring only small tuning in between waveguide measurements. This method is used extensively in waveguide characterization.
Using a known edge reflectance coefficient (calculated using effective mode index and air index) and waveguide with unknown loss, the waveguide can be modeled as a simple lossy resonator.
The loss of this resonator depends on wavelength; sweeping the wavelength (even by a few nm) will cause a change in output power, something a high resolution Ge Photodetector can measure. The setup we used had a software connected to laser generator (a couple nm around 1550nm) and Ge photodetector; the computer program sweeps the wavelength, measures the change in power, and using a user input waveguide length (in this case 29mm) calculates a loss per cm. This loss calculated is an upper limit, modeling the reflectance coefficient numerical will result in more accurate reflectance coefficient and lower loss. The effective index reflectance method is only semi-analytical in the high confinement regime our waveguides worked in, so we expected our waveguides are actually much better. Below is the loss of the waveguides with two chips. These losses average to around 2db/cm, high but not prohibitive for a number of applications.

Wavguide #	Chip 1 (db/cm)	Chip 2 (db/cm)
1	2.02	2.1
2	2.06	2.8
3	1.75	2.2
4	1.64	1.73
5	1.78	1.75
6	1.68	2.0
7	Bad	2.08
8	Bad	1.82
9	5.7	1.75
10	2.8	1.62
11	1.78	1.96
12	BAD	1.76
13	2.0	2.0
14	1.62	
15	1.93	
16	2.7	
17	3.15	
18	1.96	
19	1,9	
20	1.83	
21	2.1	
22	1.93	
23	2.35	

6.5 FAILED MEASUREMENT ATTEMPTS
There were two previous attempts to produce and edge couple light into our waveguides before we got them working. These processes are included in our report so the SNF community can learn from our mistakes.

6.5.1 Failed Attempt #1

We only included one waveguide on our die, and did no oxide capping layer and no polishing. Always include as many waveguides as one can (while still reasonably spread out) on your chip, small damage can easily occur and destroy your only waveguide. The probability of getting a good waveguide increases with number of waveguides. Some groups are able to get good edge facets with simple cleaving, but this is an imprecise art, and is difficult to propagate a clean edge with large non-crystalline oxide layers like the ones our nitride waveguides sat on. Furthermore, oxide capping layer, although not technically necessary, protects the waveguides from chipping. This occured in our first attempt.

6.5.2 Failed Attempt #2

The second attempt had multiple waveguides per die and used CMP polishing. This seemed to not work, as chipping was sometimes near edges of our waveguides and the waveguide outputs showed a weird dotted line profile. Chipping of waveguides, especially high stress waveguides like stoichiometric silicon nitride, is very likely with moderate mechanical stresses like those in a CMP. Oxide capping layers helps protect cracks from forming during CMP.

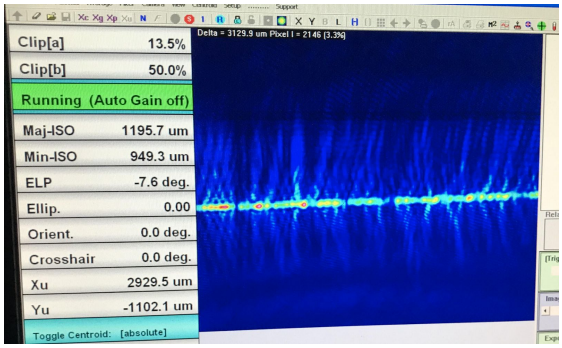

Figure 37: Output mode of waveguide from Attempt #2.

Figure 38: Broken waveguide from Attempt #1

Note: Getting a polished edge with no capping layer is possible, but it needs to be done with an expert like Tim Brand in the Ginzton Crystal Shop.

Waveguide fabrication with the Heidelberg MLA150 Maskless Aligner

Objective:

In order to make the lowest loss waveguides, we need to find a combination of dose/defocus and reflow time/temperature that gives us the best resolution and the lowest line edge roughness and line width roughness. This is done in two steps, first with software analysis of the optical characterization, we can find the dose defocus that gives us the best resolution in terms of ridges and trenches. Next, we reflow dies with PR ring structures on them. With software analysis of the SEM characterization, we can calculate how the width of rings and LER of rings change with time temperature. A reflow that reduces LER or keeps LER same while changing width or rings is useful for SNF fabrication. Finally, the best reflow time/temperature and best dose/defocus is etched and the best dose/defocus with no reflow is etched. These rings are characterized with AFM, to show how sidewall slope is affected by etching, and if width change of PR corresponds to width change of etch.

Process Flow:

Step No.	SNF/ SNSF Tool ID	Process Step
1	wbclean-res-piranha	Standard Piranha clean
2	i) thermco1 ii) thermconitride	Waveguide material stack growth (oxide growth: 280 microns followed by nitride growth: 450nm) * This step is skipped for dose/ defocus matrix of PR on Silicon.
3	YES oven	Wafer singe and prime
4	svgcoat	PR coat: 1 micron of Shipley 3612 w/o vapor prime, with 2mm EBR
5	Heidelberg	Expose desired pattern on wafer. i) Mask Layout #1: Dose/ Defocus matrix ii) Mask Layout #2: Time/ Temperature Reflow matrix using optimised dose/defocus from (i) for waveguide material stack
6	svgdev	Post exposure bake: 1 min at 110℃ Develop pattern Post develop bake: 1 min at 110℃
7	Optical microscope	i) Image ridge/ trench arrays for dose/ defocus matrix. ii) Image analysis to obtain best dose/ defocus for given substrate.
8	LaserCutter	Laser back scribing of Mask Layout #2 wafer to yield dies
9	hotplate	Reflow individual dies at different time and temperature conditions.
10	Nova SEM	i) Sputter coat with ii)Image PR rings of different widths on each time/ temperature die iii) Image analysis to find LER and LWR for each set of parameters in (i) to obtain an optimum time/ temperature value.
11	AMT-etcher	Using Recipe #4 etch waveguides after reflowing at optimum time/ temperature value
12	gasonic	PR stripping on a carrier pocket wafer using Recipe #013
13	XE-70	AFM step profile of waveguide fabricated with/ without reflow

8. REFERENCES

1. C. Shin, Variation-Aware Advanced CMOS Devices and SRAM,
   Springer Series in Advanced Microelectronics 56,
   DOI 10.1007/978-94-017-7597-7_2
2. Charmaine Chia, Joel Martis. “Grayscale lithography and resist reflow for parylene patterning”, Report submitted for E410. [https://snf.stanford.edu/SNF/processes/ee412/ee412-projects]
3. Gyorgy A. Porkolab, Paveen Apiratikul, Bohan Wang, S. H. Guo, and Christopher J. K. Richardson, "Low propagation loss AlGaAs waveguides fabricated with plasma-assisted photoresist reflow," Opt. Express 22, 7733-7743 (2014)
4. Aleksandrs Marinins, Oskars Ozolins, Xiaodan Pang, Aleksejs Udalcovs, Jaime Rodrigo Navarro,Aditya Kakkar, Richard Schatz, Gunnar Jacobsen and Sergei Popov, “Thermal reflow engineered cylindrical polymer waveguides for optical interconnects”
5. C. Shin, Variation-Aware Advanced CMOS Devices and SRAM,
   Springer Series in Advanced Microelectronics 56,
   DOI 10.1007/978-94-017-7597-7_2
6. Feidenhans'l, N. A., Taboryski, R. J., & Petersen, J. C. (2016). Optical Characterization of Nanostructured Surfaces. DTU Nanotech.
7. Surya Cheemalapati, Mikhail Ladanov, John Winskas, and Anna Pyayt, "Optimization of dry etching parameters for fabrication of polysilicon waveguides with smooth sidewall using a capacitively coupled plasma reactor," Appl. Opt. 53, 5745-5749 (2014)
8. M. Borselli, T. Johnson, and O. Painter, “Beyond the Rayleigh scattering limit in high-Q silicon microdisks: theory and experiment.” Optics express, vol. 13, no. 5, pp. 1515–1530, 2005.
9. B. P. Downey, D. J. Meyer, R. Bass, D. S. Katzer, and S. C. Binari, “Thermally reflowed ZEP 520A for gate length reduction and profile rounding in T-gate fabrication,” Journal of Vacuum Science & Technology B: Microelectronics and Nanometer Structures, vol. 30, no. 5, p. 051603, 2012. [Online].
10. Z. D. Popovic, R. A. Sprague, and G. A. N. Connell, “Technique for monolithic fabrication of microlens arrays,”Appl. Opt. 27, 1281–1288 (1988).